Journal of Pharmaceutical and Biomedical Analysis 239 (2024) 115902

Contents lists available at ScienceDirect

Journal of Pharmaceutical and Biomedical Analysis

journal homepage: www.journals.elsevier.com/journal-of-pharmaceutical-and-biomedical-analysis

Sigma receptor and aquaporin modulators: chiral resolution, configurational assignment, and preliminary biological profile of RC752 enantiomers

Roberta Listro [a], Annamaria Marra [a], Valeria Cavalloro [b], Giacomo Rossino [a], Pasquale Linciano [a], Daniela Rossi [a], Emanuele Casali [c], Marco De Amici [d], Giuseppe Mazzeo [e], Giovanna Longhi [e], Marco Fusè [e], Giulio Dondio [f], Giorgia Pellavio [g], Umberto Laforenza [g], Dirk Schepmann [h], Bernhard Wünsch [h,i], Simona Collina [a,*]

[a] Department of Drug Sciences, University of Pavia, Via Taramelli 12, 27100 Pavia, Italy
[b] Department of Earth and Environmental Sciences, University of Pavia, Via Sant 'Epifanio 14, 27100 Pavia, Italy
[c] Department of Chemistry, University of Pavia, Via Taramelli 12, 27100 Pavia, Italy
[d] Department of Pharmaceutical Sciences, University of Milan, Via Luigi Mangiagalli 25, 20133 Milan, Italy
[e] Department of Molecular and Translational Medicine, University of Brescia, Viale Europa 11, 25123 Brescia, Italy
[f] Aphad SrL, Via della Resistenza, 65, Buccinasco 20090, Italy
[g] Department of Molecular Medicine, Human Physiology Unit, University of Pavia, 27100 Pavia, Italy
[h] Westfälische Wilhelms-Universität Münster, Institut für Pharmazeutische und Medizinische Chemie, Corrensstraße 48, Münster D-48149, Germany
[i] Institut für Pharmazeutische und Medizinische Chemie, Universität Münster, Corrensstraße 48, 48149 Münster, Germany

ARTICLE INFO

Keywords:
SRs
Chiral resolution
HPLC
SFC
Absolute configuration assignment
Receptor affinity
Metabolic stability
Aquaporin

ABSTRACT

The key role of chiral small molecules in drug discovery programs has been deeply investigated throughout last decades. In this context, our previous studies highlighted the influence of the absolute configuration of different stereocenters on the pharmacokinetic, pharmacodynamic and functional properties of promising Sigma receptor (SR) modulators. Thus, starting from the racemic SR ligand **RC752**, we report herein the isolation of the enantiomers via enantioselective separation with both HPLC and SFC. After optimization of the eco-sustainable chiral SFC method, both enantiomers were obtained in sufficient amount (tens of mg) and purity (*ee* up to 95%) to allow their characterization and initial biological investigation. Both enantiomers a) displayed a high affinity for the S1R subtype ($K_i = 15.0 \pm 1.7$ and 6.0 ± 1.2 nM for the (*S*)- and (*R*)-enantiomer, respectively), but only negligible affinity toward the S2R (> 350 nM), and b) were rapidly metabolized when incubated with mouse and human hepatic microsomes. Furthermore, the activity on AQP-mediated water permeability indicated a different functional profile for the enantiomers in terms of modulatory effect on the peroxiporins gating.

1. Introduction

In the drug discovery and/or chemical biology scientific fields, researchers are often focused on the investigation of new chiral small molecules endowed with biological activity. [1] In these contexts, besides the interaction with biological targets, including transporters, membrane lipids, and enzymes, that shapes the ligand pharmacodynamic profile, the pharmacokinetic features of the most promising isomers should be carefully explored. Indeed, during the ADMET (Absorption-Distribution-Metabolism-Elimination-Toxicity) profiling step of drug discovery, putative differences in the pharmacokinetic properties among individual enantiomers/stereoisomers are routinely evaluated.[2].

In the last years, our research group has been studying in-depth Sigma receptors (SRs) and their modulation by chiral small molecules, which were characterized in terms of pharmacodynamic as well as pharmacokinetic properties. The two SR subtypes, Sigma 1 (S1R) and Sigma 2 (S2R), are involved in cell survival and control various critical functions in the human body. [3,4] S1Rs are expressed in the central nervous system (CNS), and their agonists or positive modulators are

* Corresponding author.
E-mail address: simona.collina@unipv.it (S. Collina).

https://doi.org/10.1016/j.jpba.2023.115902
Received 30 October 2023; Received in revised form 30 November 2023; Accepted 1 December 2023
Available online 4 December 2023

potentially useful in the treatment of depression, schizophrenia, Parkinson's and Alzheimer's diseases, and acute/chronic neurodegenerative diseases involved also in pain control.[5,6] On the other hand, S1R ligands with an antagonist profile showed promising activity in treating different tumor cell lines.[7] Indeed, S2Rs are overexpressed in tumor cells and tissues in proliferation and S2R ligands can promote toxic damages, which trigger autophagy or cell-cycle arrest phenomena.[8,9] Thus, compounds with a pan activity, i.e., a balanced S1R antagonist and S2R agonist profile, may counteract tumor diseases. On these premises, our ongoing interest in this research field aims at refining the properties of novel ligands, in particular chiral derivatives, to better define the therapeutic potential of SR modulators. In this respect, the previously identified hit compound (*E*)-**RC106** was characterized by a relevant pan profile coupled with a promising activity in a panel of cancer cell lines (Fig. 1).[10–12] Conversely, a modification of the aromatic moiety and hydrogenation of the double bond resulting in a chiral ligand affected the ligand's profile, as exemplified by compound (±)-**RC33** that became an S1R agonist with a potential activity towards neurodegenerative diseases.[13] Furthermore, replacement of the methyl with the hydroxymethyl group at the stereogenic center imparted to the new ligand (±)-**RC752** high selectivity towards the S1R subtype with a concomitant shift, from agonist to antagonist, of the pharmacological profile, thus engendering a specific activity against neuropathic pain.[14].

These chiral derivatives, and other related structurally modified analogues, proved that SRs are prone to discriminate between enantiomers. Moreover, a different behavior of the ADMET profile of enantiomeric pairs was observed. However, enantiomers do not always have a different binding affinity towards SRs. For instance, the interaction of the two enantiomers of **RC33** with SRs is non-stereoselective, as they display comparable affinities and equal effectiveness as S1R agonists without observable toxic effects. On the other hand, when hepatic metabolic stability assays were performed, (*S*)-**RC33**, at variance with its enantiomer, showed a preference for oxidative metabolic processes in the presence of NADPH in both rat and human microsomes, highlighting a degree of pharmacokinetic enantio-discrimination.[14–16].

Since predictions on the role of molecular chirality for this group of structurally related SR ligands are not easy to draw, we planned to isolate and characterize **RC752** enantiomers to explore how chirality influences the biological profile. The known methods to prepare enantiomerically pure compounds include chiral resolution of racemates, use of chiral pool building blocks, asymmetric synthesis, and enantioselective high-performance liquid chromatography (HPLC) on chiral Stationary Phases (CSPs). In this work, we experimented the latter approach since it is suitable for achieving both enantiomers with high enantiomeric purity and in sufficient amounts for the initial biological screening. In addition to HPLC, we explored Supercritical Fluid Chromatography (SFC), which is a quite versatile technique, given also its intrinsic eco-sustainable properties. Indeed, in the last years, the application of the SFC approach was extended also to industrial scale separations of chiral ligands.[17,18].

Aquaporins (AQPs) are a transmembrane protein family facilitating the osmotically driven diffusion of water.[19] In addition to water, AQPs are permeable to small solutes as glycerol, urea, ammonia and hydrogen peroxide (H_2O_2). Recently, a subset of AQPs (AQP0, AQP1, AQP3, AQP5, AQP6, AQP8, AQP9, and AQP11) showed a marked permeability to H_2O_2 and for this reason they were named peroxiporins.[20,21] Due to their ability to facilitate H_2O_2 diffusion, peroxiporins may have a beneficial effect in oxidative stress through a ROS scavenging mechanism. We have screened the effect of some small molecules on the AQP-mediated water permeability of HeLa cells in the presence of oxidative stress conditions.[22] The results suggested that SRs may control the pore gating peroxiporins and their related physiological functions.

The previous work extensively explored the potential of the racemate in addressing challenging pathological conditions such as neuropathic pain. This study aims at advancing further our biological characterization by introducing an additional layer of investigation - i.e., evaluating the individual actions of the two enantiomers in comparison to the racemate. Therefore, we prepared the enantiomers of **RC752**, assigned their absolute configuration by means of chiroptical techniques, and evaluated their affinity at on SR subtypes and their activity in influencing the AQP-mediated diffusional water permeability. This latter effect is an index of the H_2O_2 permeability, whose modulation by AQP may represent a valuable tool to control the cellular redox state.

2. Materials and methods

2.1. High-performance liquid chromatography

Chromatographic resolution was carried out at room temperature on a Jasco (Tokyo, Japan) system consisting of a PU-1580 pump and MD-1510 photodiode array (PDA) detector. Chromatogram acquisitions and elaborations were performed using the ChromNAV software (Tokyo, Japan). The resolution factor was directly given by the software, while the selectivity factor (α) was calculated.

The best enantiomeric resolution was achieved exploiting Chiralpak IC® column (4.6 × 250 mm, 5 μm); mobile phase: Heptane/EtOH/DEA/TFA (90:10:0.1:0.3); flow rate: 1 mL min^{-1}; sample concentration: 1 mg mL^{-1}; injection volume: 10 μL. A Hamilton (Reno, NV, USA) syringe (syringe volume: 2.5 mL; loop: 1 mL) was employed for (semi)-preparative chiral resolutions. In detail, the scale-up of the analytical conditions allowed us to set up the following method: Column: Chiralpak IC® (10 × 250 mm, 5 μm); mobile phase: Heptane/EtOH/DEA/TFA (90:10:0.1:0.3); flow rate: 4 mL min-1; sample concentration: 4 mg mL^{-1}; injection volume: 1 mL. Results are expressed as retention factors (k_1 and k_2), and selectivity (α) and resolution (R_S) factors.

2.2. Supercritical fluid chromatography

A JASCO SFC-4000 Analytical SFC system was used, equipped with CO_2 supercritical phase pump, a backpressure regulator and temperature-controlled column oven. The polar co-solvent was IPA. The HPLC system was provided with specific SFC-resistant enantiopure stationary phase columns (Chiralpak IA®,10 × 250 mm, 5 μm).

2.3. Specific optical rotation

Optical rotatory power values were measured on a Jasco photoelectric polarimeter DIP 1000 (Tokyo, Japan). Analyses were conducted using a 0.5 dm cell, methanol (MeOH) as solvent, a 0.25% concentration, and a sodium lamp (λ = 589 nm).

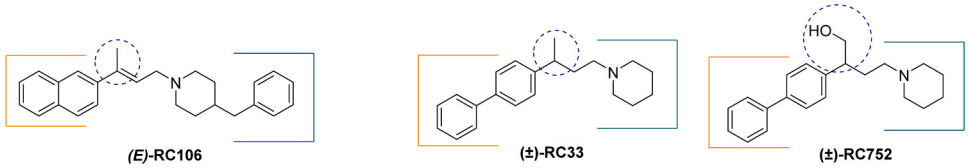

Fig. 1. Structural similarities and differences among three SRs ligands identified by our research group.[11,13,14].

2.4. Absolute configuration assignment

Vibrational Circular Dichroism (VCD) measurements were conducted using a Jasco FVS 6000 FTIR instrument equipped with a ZnSe photoelastic modulator (PEM), working at 50 kHz modulation, placed past a wire grid linear polarizer and with lock-in amplifier after detection, with an MCT liquid-N_2 cooling device for the regions 850–2000 cm^{-1}. Solutions of (±)-**RC752** in deuterated chloroform with 0.09 M concentration were prepared and VCD spectra were recorded in a 200 μm BaF_2 cell. 5000 scans were acquired, and a similar spectrum was taken for the solvent and subtracted out. Electronic Circular Dichroism (ECD) measurements were conducted with the use of a Jasco 815SE instrument with samples dissolved in acetonitrile at 0.0035 M concentration in 0.1 mm quartz cuvette. 10 scans were acquired. ECD spectra of the solvent were recorded in the same conditions and subtracted thereafter from the sample ECD spectra. UV spectra were obtained from the same apparatus. DFT and TD-DFT calculations were performed by use of Gaussian16 program22 preceded by a conformational search performed with the CREST program17. The configuration was set to (*R*)- for all calculations. B3LYP/TZVP with an empirical dispersion (D3BJ) level of theory was employed for DFT and CAM-B3LYP/TZVP for TD-DFT calculations. The polarizable continuum model (PCM) approximation was employed as solvent model for both chloroform and acetonitrile.

2.5. Receptor binding studies

Guinea pig brains are commercially available (Harlan-Winkelmann, Borchen, Germany). Homogenizers: Elvehjem Potter (B. Braun Biotech International, Melsungen, Germany) and Soniprep® 150 (MSE, London, UK). Centrifuges: cooling centrifuge model Eppendorf 5427 R (Eppendorf, Hamburg, Germany) and high-speed cooling centrifuge model Sorvall® RC-5 C plus (Thermo Fisher Scientific, Langenselbold, Germany). Multiplates: standard 96-well multiplates (Diagonal, Muenster, Germany). Shaker: self-made device with adjustable temperature and tumbling speed (scientific workshop of the Pharmazeutische und Medizinische Chemie Institute). Harvester: MicroBeta® FilterMate 96 Harvester. Filter: Printed Filtermat Typ A and B. Scintillator: Meltilex® (Typ A or B) solid state scintillator. Scintillation analyzer: MicroBeta® Trilux (all Perkin Elmer LAS, Rodgau-Jügesheim, Germany). The preparation of membrane homogenates from guinea pig brain and the S1R binding assay protocol adopted were already published.[14].

2.5.1. Sigma receptor assay

The assay was performed with the radioligand [^{3}H]-(+)-pentazocine (22.0 Ci/mmol; Perkin Elmer). The thawed membrane preparation of guinea pig brain (about 100 μg of the protein) was incubated with various concentrations of test compounds, 2 nM [^{3}H]-(+)-pentazocine, and TRIS buffer (50 mM, pH 7.4) at 37 °C. The non-specific binding was determined with 10 μM unlabeled (+)-pentazocine. The K_d value of (+)-pentazocine is 2.9 nM.

2.6. Liver microsomes metabolic stability

Mouse (Sigma Aldrich, CD-1 male, pooled) and human microsomes (Sigma Aldrich, human, pooled) 0.5 mg mL^{-1} were preincubated with both **RC752** enantiomers dissolved in DMSO at 1 μM in phosphate buffer 50 mM, pH 7.4, and 3 mM $MgCl_2$ for 10 min at 37 °C. The reaction was then started by adding the cofactor mixture solution (NADP, glucose-6-phosphate, glucose-6-phosphate dehydrogenase in 2% $NaHCO_3$). Samples were taken at 0, 10, 30, 45 and 60 min and added to acetonitrile to stop the reaction (n = 3). Samples were then centrifuged, and the supernatant was analyzed by LC-MS/MS to quantify the test item. The method to evaluate the in vitro metabolic stability and the description of the analytical method were already published.[14].

2.7. AQP-mediated water permeability measurements

Osmotic water permeability was assessed in HeLa cells suspension by the stopped-flow light scattering method as previously described.[13] The experiments were performed at 21 °C by using the RX2000 stopped flow apparatus (Applied Photophysics, Leatherhead, UK) with a pneumatic drive accessory (DA.1, Applied Photophysics) coupled with a Varian Cary 50 spectrometer (Varian Australia Pty Ltd., Australia). Scattered light intensity with a dead time of 6 ms was recorded at a wavelength of 450 nm. Cells were exposed to the hypotonic gradient of 150 mosm/L and the time course of cell swelling was measured for 60 s at the acquisition rate of one point/0.0125 s. The initial rate constant of cell volume changes (k) was obtained by setting the time course light scattering with a single exponential equation (GraphPad Prism 4.00, 2003).

To evaluate the antioxidant effect of the test compounds on water permeability, HeLa cells were divided into different groups: (1) controls, cells left at room temperature (21 °C) in the presence of MeOH at the same concentration than treated cells; (2) heat-stressed cells, cells heat-treated by placing them in a water thermostatic and shacking bath at 42 °C for 3 h; (3) heat-stressed cells pre-treated, cells heat-stressed in the presence of **RC752** (enantiomers and racemate) at 20 μM final concentration (dissolved in MeOH). Moreover, to test the possible capacity of the molecules to affect the AQP gating in eustress condition, HeLa cells were incubated with or without the compounds at 21 °C for 3 h.

3. Results and discussion

3.1. Chiral resolution

We selected enantioselective HPLC and SFC as viable strategies for rapid access to both **RC752** enantiomers with high enantiomeric purity and in reasonable amounts. Four chiral stationary phases differing in the polysaccharide backbone (cellulose or amylose), the acyl moiety at the backbone, the nature of the CSP binding (coated or immobilized), and the elution mode were evaluated (Table SI-2). They are routinely used in both enantioselective HPLC and SFC applications, with SFC often being the most effective for chiral separations thanks to the higher flow rates adopted, able to reduce the elution time. The CSPs used in the present work are reported in Table1.

Firstly, an HPLC screening elution protocol was applied on an analytical scale in both normal phase (NP) and reverse phase (RP) elution mode. For the NP elution, various combinations of *n*-heptane (Hept) and ethanol (EtOH) as polar modifier have been applied, whereas, in the RP elution mode, pure EtOH or methanol (MeOH) as eluents have been experimented. Moreover, diethylamine (DEA, 0.1%) was added to the mobile phase for the coated CSPs and a mixture of DEA (0.1%) and trifluoroacetic acid (TFA, 0.3%) for the immobilized CSPs. In such a way, the experimental conditions yielding the best enantiodiscrimination, have been identified and then were properly tailored to the (semi)-preparative scale.[23–25].

Secondly, SFC elution conditions have been experimented. In this case, the mobile phase was prevalently composed by CO_2 as the supercritical fluid. CO_2 has no toxic effect and has eluting properties comparable with those of *n*-hexane. [26] For the compound elution, CO_2 was used with a co-solvent such as MeOH, EtOH, isopropyl alcohol (IPA) or ACN, with a maximum 3:2 ratio between supercritical fluid and polar modifiers. Moreover, different acids (HCOOH, CH_3COOH and TFA) or bases (Diethylamine, DEA) additive could be added. The screening of mobile phases was reported in Table SI-1.

Poor results in terms of peak separation were obtained with conventionally coated CSPs. On the other hand, immobilized columns gave satisfying outcomes concerning peak separation, peak shape and enantioselectivity. In general, immobilized columns exhibited favorable outcomes with high concentrations of non-polar mobile phases (*n*-hexane and *n*-heptane showed comparable results) and low percentages of

polarity modifiers (such as ethanol or IPA), resulting in effective peak separations. However, as the alcohol percentage increased, the method efficiency decreased, and peak resolution was compromised.

Interestingly, a different behavior was observed with amylose-based chiral columns and cellulose-based ones using HPLC and SFC. Regarding HPLC, with cellulose-based chiral columns we reached the best results for the separation of (±)-**RC752.** The most efficient enantio-discrimination, characterized by short retention times (tr_1 = 16.7 min; tr_2 = 19.2 min) and baseline separation ($\alpha = 1.18$; $R_S = 2.61$), was achieved with Chiralpak™ IC as CSP and eluting with n-Hex/EtOH/DEA/TFA (90:10:0.1:0.3) (Fig. 2 and Table 1).

Differently, with SFC the resolution obtained by amylose- based CSPs showed the most satisfying results. Initially, a rapid analytical method was developed with a screening of supercritical fluid (CO_2) mixtures with different polar modifiers (co-solvents: MeOH, EtOH, IPA + 0.1% DEA) as mobile phases (Table SI-3). Therefore, explorative gradient analysis was performed, thus identifying the best experimental conditions for an isocratic elution. Chiralpak™ IA was the best performing CSP for SFC eluting with 60% of CO_2 and 40% of EtOH/Heptane/DEA (90:10:1). An optimal separation ($\alpha = 1.30$; $R_S = 2.85$) in short retention time (tr_1 = 6.5 min; tr_2 = 8.3 min) was achieved (Table 1).

Both experimental conditions were then properly scaled up to a semipreparative separation. For HPLC, 77 mg of (±)-**RC752** were processed in 20 cycles on Chiralpak IC™ column and properly fractionated according to the UV trace (Figure SI-1), affording 19 mg of the first eluted enantiomer {$[\alpha]_D = +17.9$ (c 0.25, MeOH), *ee* = 98.9%}, and 24 mg of the second eluted one {$[\alpha]_D = -16.4$ (c 0.25, MeOH), *ee* = 94.9%}, together with 31 mg of an intermediate fraction as a mixture of the two enantiomers. Regarding SFC, the already optimized conditions were easily scaled-up, using a semipreparative Chiralpak™ IA column and enhancing the flow rate from 4 mL min^{-1} to 10 mL min^{-1}.

7 cycles on the Chiralpak IA™ column were performed to process 25 mg of (±)-**RC752**. The racemate was properly fractionated in 8.8 and 9.2 mg, the first and second eluted fractions, respectively. Thus, enantiomers were obtained in sufficient amount and with adequate enantiomeric excess (*ee* > 98%) for the following characterization, i.e., the optical rotatory power assessment and the preliminary biological evaluation of individual enantiomers (Figure SI-1). The $[\alpha]_D$ values corresponded to those from the previous enantioselective HPLC analysis (Table 1).

As expected, advantages over the HPLC procedure were experienced with the application of the SFC method to the same enantio-separation, since the overall time of analysis was about halved, and the amounts of hazardous solvents were significantly reduced. The advantages of SFC over HPLC were assessed by measuring the weight of enantiomers isolated per unit of time and solvent consumption. The SFC method allowed to isolate 0.44 mg of first eluted enantiomer per minute, with a total consumption of 63.6 mL of solvent per mg of first isolated fraction. Conversely, the HPLC method provided 0.23 mg per minute of the first fraction and consumed 116.1 mL of solvents per mg of first isolated enantiomer. Moreover, a slight improvement of the enantiomeric purities was attained by applying the SFC technique.

3.2. Absolute configuration assignment

The absolute configuration (AC) of the HPLC separated fractions of (±)-**RC752** to either (*R*)-(—) or (*S*)-(+) was assigned by a combination of chiroptical spectroscopic methods: VCD and ECD. Theoretical spectra were simulated in the framework of the density functional theory (DFT) and its time-dependent extension (TD-DFT).[27–29] Experimental VCD and IR spectra of the two eluted fractions of (±)-**RC752**, namely (+)-**RC752** and (—)-**RC752**, were recorded in deuterated chloroform ($CDCl_3$) solutions at about 0.09 M concentration (see Figure SI-2). The conformational space of the (*R*)-enantiomer was explored through the CREST program.[30] The collected geometries were then re-optimized at the DFT level of theory, providing six conformers within a 2 kcal/mol energy interval with respect to the global minimum (see Figure SI-2 and Table SI-4). The four most populated conformers (covering about 96% of the overall population) were then utilized to predict the VCD-IR spectra. In Fig. 3, we report the experimental spectrum of (—)-**RC752** (obtained as the semi-difference of (—) and (+) experimental spectra) and the calculated (*R*)-**RC752** spectrum. Despite some mismatching in the relative intensity evaluation of the doublets at ca. 1050 cm^{-1} and 1350 cm^{-1} and the slight overestimation of the intensity of the band labeled 7 at ca. 1500 cm^{-1}, the calculated IR spectrum satisfactorily predicted the experimental one.

For a better matching of experimental and calculated VCD spectra, we employed the similarity indices (namely, S.I. and SimNN) approach.[28,31] The harmonic approximation is known to overestimate the transition energies, thus, for a better comparison, the predicted VCD-IR spectra were shifted in energies employing "arbitrary" scaling factors.[32] Maximizing the S.I. allows to search for the best scaling factor to be applied to the computed spectra. These indices vary between 0 e 1 for IR (1 means perfect matching between experimental and calculated spectra) and between − 1 (reversed AC assignment should be made) and + 1 (perfect AC assignment has been made) for VCD. In Table SI-5 we report S.I. and SimNN values, calculated applying different scaling factors, thus showing that using a single scaling factor does not provide a satisfactory matching. Therefore, VCD and IR spectra were examined separately in the two different ranges: from 950 to 1220 cm^{-1} and from 1220 to 1650 cm^{-1}. The best S.I. scaling factor was found to be 0.98 for 950–1220 cm^{-1} and 0.97 for the 1220–1650 cm^{-1} range. The scaling factors optimized on the IR spectrum were then employed to compare experimental and calculated VCD spectra: S.I. is + 0.18 (SimNN is +0.09) for 0.98 scaling factor (950–1220 cm^{-1} range) and + 0.26 (SimNN is +0.14) for 0.97 (1220–1650 cm^{-1} range). We also evaluated

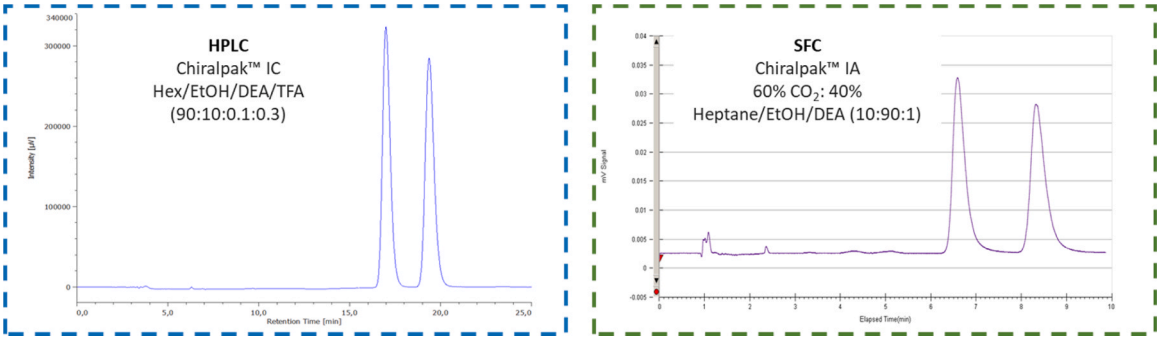

Fig. 2. On the left: analytical HPLC-UV trace (λ = 254 nm) of (±)-**RC752**. Column: Chiralpak™ IC (4.6 × 250 mm, 5 μm); mobile phase: n-Hex/EtOH/DEA/TFA (90:10:0.1:0.3); flow rate: 1 mL min^{-1}; sample concentration: 1 mg mL^{-1}; injection volume: 10 μL. On the right: chromatographic profile in analytical scale SFC-UV trace (λ = 254 nm) of (±)-**RC752**. Column: Chiralpak IA® (4.6 × 250 mm, 5 μm); mobile phase: Heptane/EtOH/DEA (10:90:1) at 40% concentration in CO_2; temperature: 40 °C, flow rate: 4 mL min^{-1}; sample concentration: 1 mg mL^{-1}; injection volume: 10 μL.

Table 1
Results of the selected elution protocol in HPLC and SFC for (±)-**RC752**.

	Eluted	Column	Eluent (v/v/v/v)	k	α	R_s	N° of theoretical plates	$[\alpha]_D$	ee%
HPLC	First	Chiralpak™ IC	Hex/EtOH TFADEA 90:10:0.1:0.3	3.6	1.18	2.61	38376	+ 17.9	98.9
	Second			4.3			34430	-16.4	94.9
SFC	First	Chiralpak™ IA	60% CO2:40% Hep/EtOHDEA 10:90:1	5.8	1.30	2.85	2317	+ 17.9	98.8
	Second			7.7			2608	-17.2	98.2

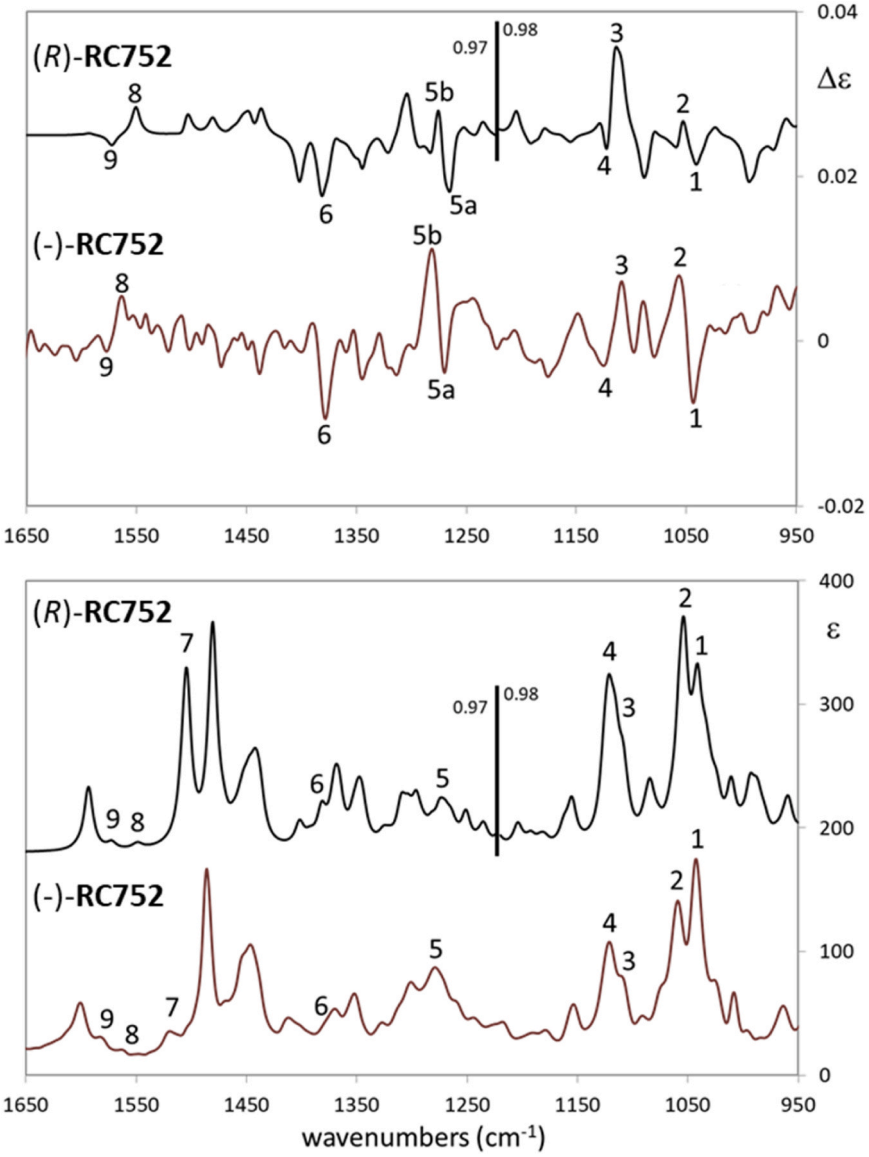

Fig. 3. Comparison of calculated and experimental VCD-IR spectra of (±)-**RC752**. The experimental spectrum (in dark red) for (—)-**RC752** and the calculated spectrum (in black) for (*R*)-**RC752** are reported. The experimental spectrum was measured in $CDCl_3$ solution at ca. 0.09 M concentration and is reported as semi-difference between the second eluted (—)-**RC752** and the first eluted (+)-**RC752** enantiomer (see Figure SI-2). Calculations were performed at the DFT/B3LYP/TZVP/PCM level (chloroform) with empirical dispersion functions. Calculated spectra were reported as weighed average (according to ΔG free energies) over the first four most populated conformers (see Figure SI-2 and Table SI-4) with arbitrarily assigned (*R*)- AC. Vertical thick black bar at 1220 cm^{-1} separates the two computed spectral ranges (950–1220 cm^{-1} and 1220–1650 cm^{-1}), in which different scaling factors (vide infra) were applied (0.98 and 0.97, respectively).

S.I. between the (—)-**RC752** experimental spectrum and the (*S*)-**RC752** enantiomer which, as expected, turned to negative values. Despite non-perfect experimental-computational matching, it can be noted (Figure SI-3) that the (*R*)- AC satisfactorily predicted the main experimental (—)-**RC752** VCD features, from low to high wavenumbers: the negative/positive doublet 1/2 at ca. 1050 cm^{-1}, the positive/negative bands 3 and 4, the negative/positive doublet 5a/5b, the negative band 6 and the weak doublet 8/9 (Fig. 3). A thorough investigation of each conformer VCD-IR calculated spectrum (see Figure SI-5) allowed us to understand all contributions to the overall VCD-IR spectra and to further back up the proposed AC assignment. It is also worth noting that calculated similarity indices values increase, if related to the most populated conformer (*R*)-**RC752**, to + 0.56/+ 0.39 and to + 0.49/+ 0.32 (S.I./SimNN) according to the 950–1220 cm^{-1} and 1220–1650 cm^{-1} ranges, respectively (Table-SI2). The (—)-**RC752** ECD spectrum shows very weak positive bands corresponding to the biphenyl

A band at 250 nm and a negative centered one at ca. 200 nm (see Figure SI-4). Biphenyl torsion angle drives 250 nm ECD band sign and, according to Superchi et al.[33], a positive CD band corresponds to a preferential M torsion. TD-DFT calculations confirmed this trend showing that all P-oriented biphenyl (±)-**RC752** conformers possess positive 250 nm CD and vice-versa for the M-oriented biphenyl conformers. Weighed ECD does not correctly predict the experimental one because of free rotation of biphenyl which provided a low chiroptical response (Figure SI-6).

3.3. Biological profile

As a first step, the binding affinity of (*R*)-**RC752** and (*S*)-**RC752** to both SRs was evaluated. Both enantiomers displayed a high affinity for the S1R subtype ($K_i = 15.0 \pm 1.7$ and 6.0 ± 1.2 nM for the (*S*)- and (*R*)-enantiomer, respectively), but only negligible affinity toward the S2R (> 350 nM). Therefore, in terms of affinity, a poor enantioselectivity was observed with a slight enantio-preference for the (*R*)-configured **RC752**. The hepatic metabolic stability, of both enantiomers was determined using mouse and human hepatic microsomal fractions. Incubation of the enantiomers with these preparations represents a suitable test to evaluate their metabolic stability to phase I oxidative metabolism. **RC752** and its enantiomers were highly metabolized when incubated with mouse and human hepatic microsomes. However, the (*R*)-configured enantiomer showed a tendency to be slightly less metabolized in the human species than (*S*)-**RC752** (10.9 min, 6.1 min).

Next, the functional profile of racemic and enantiomeric **RC752** on aquaporin (AQP)-mediated water permeability was studied. AQPs include a channel-forming protein family that facilitates the diffusion of water and other small molecules through cell membranes. Some of these proteins were found to transport H_2O_2 and, for that reason, were named peroxiporins. AQP functions are thus critical to ensure reactive oxygen species (ROS) scavenging properties and cell survival.[13,34] Our research group has recently reported that S1R agonists, but not antagonists, can restore or protect AQP-mediated water and H_2O_2 permeability in heat-stressed HeLa cells, thus counteracting oxidative stress.[20] Moreover, the osmotic water permeability of AQPs was shown to be indicative of H_2O_2 permeability.[34] Heat treatment was used as a cell stressor and decreased water permeability. Water permeability was measured in heat-stressed cells incubated with or without racemic and enantiomeric **RC752**, and the values were compared to those of control cells incubated at room temperature. The stopped-flow light scattering was used to measure the osmotic water permeability of HeLa cells, and was expressed as a percent of the exponential rate constant k.

The effects of racemic and enantiomeric **RC752** were evaluated in both heat-stressed cells and in the absence of oxidative stress (Fig. 4). The racemate was unable to prevent the reduction of water permeability in both heated stressed and eustress cells conditions. The (*R*)-**RC752** was ineffective in restoring water permeability in heat-stressed cells, as well as (±)-**RC752** (Fig. 4A), according to the S1R antagonist profile, previously demonstrated by us.[13,14] Curiously, the water permeability experiments performed in HeLa cells incubated in the absence of oxidative stress at room temperature showed that the (*S*)-configured enantiomer acted as the racemate, inhibiting the water permeability (Fig. 4B). Therefore, the (*R*)-**RC752** enantiomer showed an opposite behavior in stressed and eustress conditions.

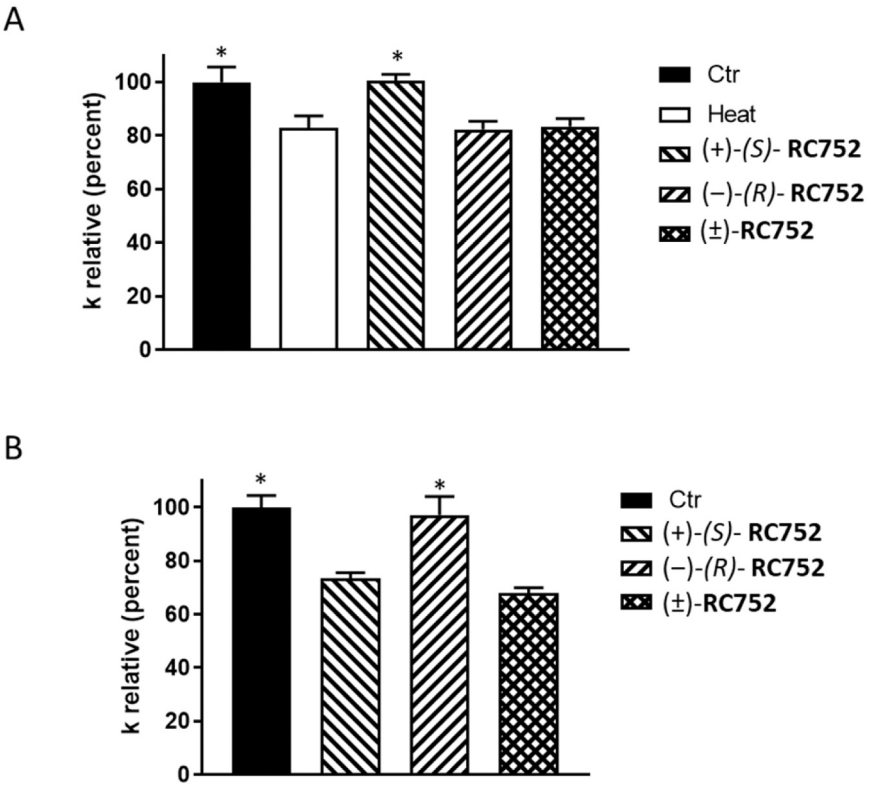

Fig. 4. A) Effect of (+)-(*S*)-**RC752**, (—)-(*R*)-**RC752**, and the racemate (±)-**RC752** on water permeability of Hela cells in normal and heat-stress conditions. Three different conditions were considered: (1) untreated cells incubated at r.t. (Controls, Ctr); (2) cells treated at 42 °C for 3 h (heat-stressed, Heat); (3) heat-stressed cells pre-treated with the enantiomers and racemate at 20 μM final concentration. (**B**) The effect of the compounds on water permeability independently on their antioxidant properties was measured in HeLa cells treated at 21 °C for 3 h with single compounds at 20 μM final concentration. Bars represent the osmotic water permeability of HeLa cells expressed as a percent of the exponential rate constant k. Values are means ± SEM of 4–15 single shots (time course curves) for each of 4–6 different experiments. A) * , $P < 0.05$ vs. Heat, (—)-(*R*)-**RC752**, (±)-**RC752** (ANOVA, followed by Newman-Keuls's *Q* test). B) * , $P < 0.05$ vs. (+)-(*S*)-**RC752** and (±)-**RC752** (ANOVA, followed by Newman-Keuls's *Q* test).

4. Conclusions

As a continuation of our efforts in investigating SRs and their ligands, in this study we report on the isolation of the enantiomeric pair of derivative **RC752**, whose racemate had been previously characterized as an SR antagonist by our research group. The two enantiomers were obtained in very high enantiomeric purity (*ee* $\geq$ 95%) through enantioselective HPLC and SFC. Due to the shorter analysis times, the overall greener procedure, and the slightly better results in terms of enantiomeric purity of the analytes, SFC was found to be the most convenient method.

With respect to S1R binding and the metabolic stability, a slight enantio-preference for (*R*)-**RC752** enantiomer was detected. Unexpectedly, preliminary results showed that the two enantiomers exert different modulatory effects on the peroxiporins gating, depending on eustress and stress conditions. It has been hypothesized that oxidative stress conditions may lead to the oxidation of cysteine residues of the AQPs thus inducing a conformational change.[35] Our hypothesis is that these different conformations of AQP may influence the interaction with the protein, causing a different activity of the two enantiomers. These data on the effect of **RC752** enantiomers on AQP should be considered as preliminary results, and the~~ir~~ interaction of these SR1 ligands will be clarified by further studies. Thus, even when enantiomers seem to behave similarly, a deeper exploration reveals a distinct behavior, providing the foundation for subsequent, more in-depth investigations.

CRediT authorship contribution statement

Roberta Listro: Writing - Original Draft, Methodology, Investigation, Validation. **Annamaria Marra**: Methodology, Investigation. **Valeria Cavalloro**: Investigation, Writing - Original Draft, Visualization. **Giacomo Rossino**: Investigation, Writing - Original Draft, Visualization. **Pasquale Linciano**: Supervision, Methodology **Daniela Rossi**: Supervision, Methodology. **Emanuele Casali**: Investigation. **Marco De Amici**: Supervision, Writing - Review & Editing, Visualization. **Giuseppe Mazzeo**: Methodology, Investigation. **Giovanna Longhi**: Methodology, Validation. **Marco Fusè**: Investigation. **Giulio Dondio**: Methodology, Investigation, Resources. **Giorgia Pellavio**: Methodology, Investigation. **Umberto Laforenza**: Supervision, Methodology **Dirk Schepmann**: Methodology, Investigation. **Bernhard Wünsch**: Supervision, Writing - Review & Editing. **Simona Collina**: Writing - Review & Editing, Project administration, Conceptualization, Supervision.

Declaration of Competing Interest

The authors declare the following financial interests/personal relationships which may be considered as potential competing interests: Simona Collina reports was provided by University of Pavia. If there are other authors, they declare that they have no known competing financial interests or personal relationships that could have appeared to influence the work reported in this paper.

Acknowledgement

This work was supported by the European Union – PON R&I 2014–2020-Asse IV “Istruzione e Ricerca per il recupero-REACT-EU”, Azione IV.6 “Contratti di Ricerca su tematiche Green.

Appendix A. Supporting information

Supplementary data associated with this article can be found in the online version at doi:10.1016/j.jpba.2023.115902.

References

[1] S.T. Toenjes, J.L. Gustafson, Atropisomerism in medicinal chemistry: challenges and opportunities, Future Med Chem. 10 (2018) 409–422, https://doi.org/10.4155/fmc-2017-0152.
[2] V.V.S. Kumari Rayala, J.S. Kandula, et al., Advances and challenges in the pharmacokinetics and bioanalysis of chiral drugs, Chirality 34 (2022) 1298–1310, https://doi.org/10.1002/chir.23495.
[3] T. Maurice, T.-P. Su, The pharmacology of sigma-1 receptors, Pharm. Ther. 124 (2009) 195–206, https://doi.org/10.1016/j.pharmthera.2009.07.001.
[4] D. Crottès, H. Guizouarn, P. Martin, F. Borgese, O. Soriani, The sigma-1 receptor: a regulator of cancer cell electrical plasticity? Front. Physiol. 4 (2013). ⟨https://www.frontiersin.org/article/10.3389/fphys.2013.00175⟩ (accessed January 14, 2022).
[5] G. Rossino, M. Rui, P. Linciano, D. Rossi, M. Boiocchi, M. Peviani, E. Poggio, D. Curti, D. Schepmann, B. Wünsch, M. González-Avendaño, A. Vergara-Jaque, J. Caballero, S. Collina, Bitopic sigma 1 receptor modulators to shed light on molecular mechanisms underpinning ligand binding and receptor oligomerization, J. Med Chem. 64 (2021) 14997–15016, https://doi.org/10.1021/acs.jmedchem.1c00886.
[6] G. Rossino, M. Rui, L. Pozzetti, D. Schepmann, B. Wünsch, D. Zampieri, G. Pellavio, U. Laforenza, S. Rinaldi, G. Colombo, L. Morelli, P. Linciano, D. Rossi, S. Collina, Setup and validation of a reliable docking protocol for the development of neuroprotective agents by targeting the Sigma-1 Receptor (S1R), Int. J. Mol. Sci. 21 (2020) 7708, https://doi.org/10.3390/ijms21207708.
[7] S. Collina, E. Bignardi, M. Rui, D. Rossi, R. Gaggeri, A. Zamagni, M. Cortesi, A. Tesei, Are sigma modulators an effective opportunity for cancer treatment? A patent overview (1996-2016), Expert Opin. Ther. Pat. 27 (2017) 565–578, https://doi.org/10.1080/13543776.2017.1276569.
[8] C. Zeng, S. Vangveravong, J. Xu, K.C. Chang, R.S. Hotchkiss, K.T. Wheeler, D. Shen, Z.-P. Zhuang, H.F. Kung, R.H. Mach, Subcellular localization of sigma-2 receptors in breast cancer cells using two-photon and confocal microscopy, Cancer Res 67 (2007) 6708–6716, https://doi.org/10.1158/0008-5472.CAN-06-3803.
[9] U.B. Chu, T.A. Mavlyutov, M.-L. Chu, H. Yang, A. Schulman, C. Mesangeau, C. R. McCurdy, L.-W. Guo, A.E. Ruoho, The Sigma-2 receptor and progesterone receptor membrane component 1 are different binding sites derived from independent genes, EBioMedicine 2 (2015) 1806–1813, https://doi.org/10.1016/j.ebiom.2015.10.017.
[10] M. Rui, D. Rossi, A. Marra, M. Paolillo, S. Schinelli, D. Curti, A. Tesei, M. Cortesi, A. Zamagni, E. Laurini, S. Pricl, D. Schepmann, B. Wűnsch, E. Urban, V. Pace, S. Collina, Synthesis and biological evaluation of new aryl-alkyl(alkenyl)-4-benzylpiperidines, novel sigma receptor (SR) modulators, as potential anticancer-agents, Eur. J. Med. Chem. 124 (2016) 649–665, https://doi.org/10.1016/j.ejmech.2016.08.067.
[11] R. Listro, S. Stotani, G. Rossino, M. Rui, A. Malacrida, G. Cavaletti, M. Cortesi, C. Arienti, A. Tesei, D. Rossi, M.D. Giacomo, M. Miloso, S. Collina, Exploring the RC-106 Chemical Space: Design and Synthesis of Novel (E)-1-(3-Arylbut-2-en-1-yl)-4-(Substituted) Piperazine Derivatives as Potential Anticancer Agents, Frontiers in Chemistry. 8 (2020). https://www.frontiersin.org/article/10.3389/fchem.2020.00495 (accessed March 16, 2022).
[12] A. Tesei, M. Cortesi, S. Pignatta, C. Arienti, G.M. Dondio, C. Bigogno, A. Malacrida, M. Miloso, C. Meregalli, A. Chiorazzi, V. Carozzi, G. Cavaletti, M. Rui, A. Marra, D. Rossi, S. Collina, Anti-tumor efficacy assessment of the sigma receptor pan modulator RC-106. A promising therapeutic tool for pancreatic cancer, Front Pharm. 10 (2019) 490, https://doi.org/10.3389/fphar.2019.00490.
[13] G. Pellavio, G. Rossino, G. Gastaldi, D. Rossi, P. Linciano, S. Collina, U. Laforenza, Sigma-1 receptor agonists acting on aquaporin-mediated H2O2 permeability: new tools for counteracting oxidative stress, Int. J. Mol. Sci. 22 (2021) 9790, https://doi.org/10.3390/ijms22189790.
[14] G. Rossino, A. Marra, R. Listro, M. Peviani, E. Poggio, D. Curti, G. Pellavio, U. Laforenza, G. Dondio, D. Schepmann, B. Wünsch, M. Bedeschi, N. Marino, A. Tesei, H.-J. Ha, Y.-H. Kim, J. Ann, J. Lee, P. Linciano, M. Di Giacomo, D. Rossi, S. Collina, Discovery of RC-752, a Novel Sigma-1 receptor antagonist with antinociceptive activity: a promising tool for fighting neuropathic pain, Pharmaceuticals 16 (2023) 962, https://doi.org/10.3390/ph16070962.
[15] A.S. Kaplitz, M.E. Mostafa, S.A. Calvez, J.L. Edwards, J.P. Grinias, Two-dimensional separation techniques using supercritical fluid chromatography, J. Sep. Sci. 44 (2021) 426–437, https://doi.org/10.1002/jssc.202000823.
[16] B. Vigani, C. Valentino, V. Cavalloro, L. Catenacci, M. Sorrenti, G. Sandri, M. C. Bonferoni, C. Bozzi, S. Collina, S. Rossi, F. Ferrari, Gellan-based composite system as a potential tool for the treatment of nervous tissue injuries: cross-linked electrospun nanofibers embedded in a RC-33-loaded freeze-dried matrix, Pharmaceutics 13 (2021) 164, https://doi.org/10.3390/pharmaceutics13020164.
[17] D. Rossi, A. Marra, M. Rui, S. Brambilla, M. Juza, S. Collina, Fit-for-purpose” development of analytical and (semi)preparative enantioselective high performance liquid and supercritical fluid chromatography for the access to a novel σ1 receptor agonist, J. Pharm. Biomed. Anal. 118 (2016) 363–369, https://doi.org/10.1016/j.jpba.2015.10.047.
[18] R. Gaggeri, D. Rossi, S. Collina, B. Mannucci, M. Baierl, M. Juza, Quick development of an analytical enantioselective high performance liquid chromatography separation and preparative scale-up for the flavonoid Naringenin, J. Chromatogr. A 1218 (2011) 5414–5422, https://doi.org/10.1016/j.chroma.2011.02.038.
[19] G.M. Preston, P. Agre, Isolation of the cDNA for erythrocyte integral membrane protein of 28 kilodaltons: member of an ancient channel family, Proc. Natl. Acad. Sci. 88 (1991) 11110–11114, https://doi.org/10.1073/pnas.88.24.11110.

[20] G. Pellavio, U. Laforenza, Human sperm functioning is related to the aquaporin-mediated water and hydrogen peroxide transport regulation, Biochimie 188 (2021) 45–51, https://doi.org/10.1016/j.biochi.2021.05.011.
[21] G. Pellavio, S. Martinotti, M. Patrone, E. Ranzato, U. Laforenza, Aquaporin-6 may increase the resistance to oxidative stress of malignant pleural mesothelioma cells, Cells 11 (2022) 1892, https://doi.org/10.3390/cells11121892.
[22] G. Pellavio, M. Rui, L. Caliogna, E. Martino, G. Gastaldi, S. Collina, U. Laforenza, Regulation of aquaporin functional properties mediated by the antioxidant effects of natural compounds, Int. J. Mol. Sci. 18 (2017) 2665, https://doi.org/10.3390/ijms18122665.
[23] V. Cavalloro, K. Russo, F. Vasile, L. Pignataro, A. Torretta, S. Donini, M.S. Semrau, P. Storici, D. Rossi, F. Rapetti, C. Brullo, E. Parisini, O. Bruno, S. Collina, Insight into GEBR-32a: chiral resolution, absolute configuration and enantiopreference in PDE4D Inhibition, Molecules 25 (2020), https://doi.org/10.3390/molecules25040935.
[24] R. Gaggeri, D. Rossi, S. Collina, B. Mannucci, M. Baierl, M. Juza, Quick development of an analytical enantioselective high performance liquid chromatography separation and preparative scale-up for the flavonoid Naringenin, J. Chromatogr. A 1218 (2011) 5414–5422, https://doi.org/10.1016/j.chroma.2011.02.038.
[25] R. Listro, G. Rossino, S. Della Volpe, R. Stabile, M. Boiocchi, L. Malavasi, D. Rossi, S. Collina, Enantiomeric resolution and absolute configuration of a chiral δ-Lactam, useful intermediate for the synthesis of bioactive compounds, Molecules 25 (2020) 6023, https://doi.org/10.3390/molecules25246023.
[26] T. Fornstedt, M. Enmark, J. Samuelsson, Method transfer in SFC from a fundamental perspective, TrAC Trends Anal. Chem. 149 (2022), 116551, https://doi.org/10.1016/j.trac.2022.116551.
[27] S. Abbate, L.F. Burgi, E. Castiglioni, F. Lebon, G. Longhi, E. Toscano, S. Caccamese, Assessment of configurational and conformational properties of naringenin by vibrational circular dichroism, Chirality 21 (2009) 436–441, https://doi.org/10.1002/chir.20616.
[28] P.L. Polavarapu, Boca Raton. Chiroptical Spectroscopy: Fundamentals and Applications, CRC Press, 2016, https://doi.org/10.1201/9781315374888.
[29] G. Mazzeo, A. Cimmino, M. Masi, G. Longhi, L. Maddau, M. Memo, A. Evidente, S. Abbate, Importance and difficulties in the use of chiroptical methods to assign the absolute configuration of natural products: the case of phytotoxic pyrones and furanones produced by *Diplodia corticola*, J. Nat. Prod. 80 (2017) 2406–2415, https://doi.org/10.1021/acs.jnatprod.7b00119.
[30] P. Pracht, F. Bohle, S. Grimme, Automated exploration of the low-energy chemical space with fast quantum chemical methods, Phys. Chem. Chem. Phys. 22 (2020) 7169–7192, https://doi.org/10.1039/C9CP06869D.
[31] E. Debie, E. De Gussem, R.K. Dukor, W. Herrebout, L.A. Nafie, P. Bultinck, A confidence level algorithm for the determination of absolute configuration using vibrational circular dichroism or raman optical activity, ChemPhysChem 12 (2011) 1542–1549, https://doi.org/10.1002/cphc.201100050.
[32] M. Fusè, G. Mazzeo, G. Longhi, S. Abbate, M. Masi, A. Evidente, C. Puzzarini, V. Barone, Unbiased determination of absolute configurations by vis-à-vis comparison of experimental and simulated spectra: the challenging case of diplopyrone, J. Phys. Chem. B. 123 (2019) 9230–9237, https://doi.org/10.1021/acs.jpcb.9b08375.
[33] S. Superchi, R. Bisaccia, D. Casarini, A. Laurita, C. Rosini, Flexible biphenyl chromophore as a circular dichroism probe for assignment of the absolute configuration of carboxylic acids, J. Am. Chem. Soc. 128 (2006) 6893–6902, https://doi.org/10.1021/ja058552a.
[34] I. Medraño-Fernandez, S. Bestetti, M. Bertolotti, G.P. Bienert, C. Bottino, U. Laforenza, A. Rubartelli, R. Sitia, Stress regulates Aquaporin-8 permeability to impact cell growth and survival, Antioxid. Redox Signal. 24 (2016) 1031–1044, https://doi.org/10.1089/ars.2016.6636.
[35] H. Hadidi, R. Kamali, A. Binesh, Investigation of the aquaporin-2 gating mechanism with molecular dynamics simulations, Proteins 89 (2021) 819–831, https://doi.org/10.1002/prot.26061.